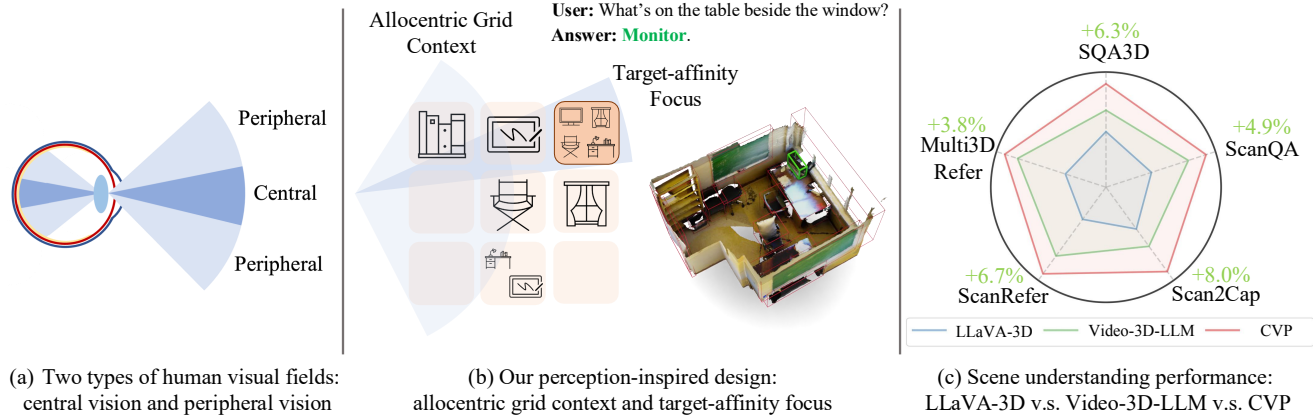


# CVP: Central-Peripheral Vision-Inspired Multimodal Model for Spatial Reasoning

Zeyuan Chen<sup>1</sup> Xiang Zhang<sup>1</sup> Haiyang Xu<sup>1</sup> Jianwen Xie<sup>2</sup> Zhuowen Tu<sup>1</sup>  
<sup>1</sup>UC San Diego <sup>2</sup>Lambda, Inc.



(a) Two types of human visual fields: central vision and peripheral vision

(b) Our perception-inspired design: allocentric grid context and target-affinity focus

(c) Scene understanding performance: LLaVA-3D v.s. Video-3D-LLM v.s. CVP

Figure 1. Overview of CVP, inspired by human visual cognition. (a) Human vision combines central vision (dark blue) for focused, high-acuity perception and peripheral vision (light blue) for broader contextual awareness. (b) Our model mimics this dual process with **target-affinity token**, guiding attention to target-relevant objects/regions, and **allocentric grid**, capturing allocentric spatial context. (c) Quantitative results across multiple 3D scene understanding benchmarks. We report EM on SQA3D [40], CIDEr on ScanQA [3] and Scan2Cap [12], Acc@0.25 on ScanRefer [7], and F1@0.25 on Multi3DRefer [70]. With target-affinity token and allocentric allocentric grid, CVP consistently outperforms state-of-the-art models such as LLaVA-3D [76] and Video-3D-LLM [74].

## Abstract

We present a central-peripheral vision-inspired framework (CVP), a simple yet effective multimodal model for spatial reasoning that draws inspiration from the two types of human visual fields – central vision and peripheral vision. Existing approaches primarily rely on unstructured representations, such as point clouds, voxels, or patch features, and inject scene context implicitly via coordinate embeddings. However, this often results in limited spatial reasoning capabilities due to the lack of explicit, high-level structural understanding. To address this limitation, we introduce two complementary components into a Large Multimodal Model-based architecture: **target-affinity token**, analogous to central vision, that guides the model’s attention toward query-relevant objects; and **allocentric grid**, akin to peripheral vision, that captures global scene context and spatial arrangements. These components work in tandem to enable structured, context-aware understanding of complex 3D environments.

Experiments show that CVP achieves state-of-the-art performance across a range of 3D scene understanding benchmarks.

## 1. Introduction

Understanding 3D scenes is a fundamental ability that agents need to have to interact with the physical world, enabling applications in robotics [19, 44, 51, 55], autonomous navigation [30, 42, 43, 48, 75], and embodied AI [18, 36, 63, 78]. Common tasks for 3D spatial understanding, such as 3D question answering (e.g. ScanQA [3], SQA3D [40]), 3D object localization (e.g. ScanRefer [7], Multi3DRefer [70]) and dense captioning (e.g. Scan2Cap [12]) all require a model to jointly reason about geometry, semantics, and spatial relationships.

The progress of Large Language Models (LLMs) [1, 16, 38, 52, 56, 57] and Large Multimodal Models (LMMs) for

images [1, 39, 52, 53] and videos [1, 4, 32, 71] has catalyzed advances in spatial intelligence. To extend these models to 3D scene understanding, one line of work [10, 20] integrates scene-level geometric representations, such as point clouds, voxels, or patch features, into LLMs via lightweight adapters, including LLaVA [39]-style projection layers or cross-attention-based modules like Q-Former [33]. These methods retain dense geometric detail and broad spatial coverage. However, mapping unordered 3D features into the token space of language models presents challenges: correspondences are often noisy, positional cues are injected implicitly through coordinates, and training can produce weak vision–language alignment due to the limited availability of labeled 3D data. Another direction [21–23] follows the egocentric perception of embodied agents, leveraging object-centric representations wherein object proposals are enriched with associated 2D and 3D features. This structure improves semantic grounding and reduces token load, but often fragments global context and under-represents inter-object spatial relationships. Most recently, researchers [74, 76] have explored using pre-trained LMMs by sampling videos present in 3D datasets and feeding the resulting frame sequences to the model. While these models achieve promising performance on various benchmarks, 3D information is typically injected only implicitly, *e.g.* via coordinate embeddings, leaving the model without an explicit, high-level allocentric representation of scene structure.

To address these limitations, we draw inspiration from the dual nature of the human visual field. Human vision consists of a high-acuity center region (fovea) and a low-acuity peripheral region. This foveal-peripheral structure allows humans to focus sharply on regions of while maintaining a broad awareness of the surrounding environment. Inspired by this efficient perceptual mechanism, several computer vision models have explored similar designs for tasks such as scene parsing [35], navigation [54], and saliency detection [50]. Mimicking this mechanism can help models allocate resources more effectively, prioritizing relevant details without losing sight of the global scene.

Motivated by this insight, we propose CVP, a framework that incorporates the following two key components designed to enhance the 3D spatial understanding ability of the base LMM model:

(1) **Target-affinity token**, which directs the model’s attention toward query-relevant objects, serving a role analogous to human central vision. This mechanism is trained with a contrastive loss, where positive samples correspond to target-relevant objects.

(2) **Allocentric grid**, which captures the global scene layout from a world-centric (allocentric) perspective, akin to peripheral vision. Object locations are discretized into a bird’s-eye-view grid, enabling structured reasoning over spatial relationships.

These two components enable CVP to reason effectively over both fine-grained object details and global spatial context. Combined with the strong pretraining of the LMM, CVP achieves state-of-the-art performance across five representative 3D scene understanding benchmarks, as illustrated in Fig. 1 (c). For example, it achieves 62.3 EM on SQA3D [40], 107.1 CIDEr on ScanQA [3], 62.0 Acc@0.25 on ScanRefer [7], and 60.2 F1@0.25 on Multi3DRefer [70], surpassing the previous state-of-the-art Video-3D-LLM by +3.7 EM, +5.0 CIDEr, +3.9 Acc@0.25, and +2.0 F1@0.25, respectively.

Our contributions are summarized as follows:

- We propose CVP, a novel framework for 3D spatial understanding, built upon the LMM model and inspired by principles of human visual perception.
- We design two complementary components to enhance spatial reasoning: (1) **target-affinity token**, which directs the model’s attention to query-relevant objects, akin to central vision; and (2) **allocentric grid**, which captures the global scene layout and spatial relationships from a world-centric perspective, resembling peripheral vision.
- Extensive experiments demonstrate that CVP achieves state-of-the-art performance on five representative 3D vision-and-language benchmarks: ScanQA, Scan2Cap, SQA3D, ScanRefer, and Multi3DRefer.

## 2. Related Work

### 2.1. 3D Scene Understanding

3D scene understanding is a fundamental problem in computer vision, with critical applications in robotics [44, 51, 55] and autonomous driving [30, 48, 75]. With the rise of large language models and large multimodal models, there has been growing interest in integrating 3D perception with natural language understanding [64, 68]. Several vision-language tasks have emerged to benchmark 3D scene understanding. In particular, 3D dense captioning [12, 28, 66] requires models to accurately localize objects and produce descriptions with accurate geometry and semantic information. 3D question answering [3, 40, 47] challenges models to interpret spatial and relational cues in the scene to answer complex queries. 3D visual grounding [7, 24, 25, 60, 70] requires models to localize objects based on free-form referring expressions. These tasks demand the joint reasoning of semantics, geometry, and spatial relationships. Some approaches utilize Bird’s Eye View (BEV) features for 3D grounding and VQA tasks [15, 59]. CVP instead adopts an allocentric grid, which is an abstract textual representation of the 3D scene that allows the language model to more effectively capture the global scene context without introducing modality misalignment. While expert models have been developed to address each of these tasks individually [2, 3, 8, 24, 27, 41, 61, 66], unified frameworks

that can handle all tasks with a single model have long been sought after. The emergence of LMMs provides a promising foundation for such generalist models, offering strong language reasoning capabilities that can be coupled with 3D scene features. Although specialized methods excel in isolated settings, there remains a clear need for a unified model capable of general-purpose 3D vision-language understanding, which is the goal we aim to achieve.

## 2.2. Large Models in 3D Scene Understanding

Recent work has demonstrated that Large Language Models (LLMs) and Large Multimodal Models (LMMs) can be extended to 3D vision–language tasks by aligning 3D representations with textual semantics. PointLLM [62] re-trains Point-BERT [64] to extract 3D embeddings and learns a projection from point-cloud features into the language space. LL3DA [10] adapts the Q-Former architecture [33] to distill point-cloud features into a set of latent tokens, which are then aligned with language via a linear mapping. Object-centric approaches [11, 21–23] utilize 3D object bounding boxes to derive instance-level embeddings, which are mapped into the language space using learned projection layers [11, 21–23] and contrastive objectives [11]. While these methods benefit from object-level semantics and category priors, they may struggle to capture holistic, scene-level spatial relationships. Another line of works [20, 74, 76] renders 3D scenes into multi-view 2D images and leverages pre-trained image encoders, such as CLIP [49], to extract multi-view features as a proxy for 3D scene representation. For example, 3D-LLM [20] aggregates multi-view features into 3D via 3D geometric cues; LLaVA-3D [76] back-projects image features into 3D space and performs 3D patch pooling; and Video-3D-LLM [74] treats rendered images as video frame sequences and injects 3D spatial information via 3D position encodings. CVP builds upon this multi-view rendering paradigm but introduces two key innovations inspired by human visual perception. At the input stage, it integrates allocentric contextual cues through a symbolic allocentric grid. At the output stage, it applies contrastive supervision via the target-affinity token aligned with target objects. Together, these enhancements promote a more structured and comprehensive understanding of complex 3D environments.

## 3. Method

Human visual perception operates through two complementary components: central vision, which enables high-acuity focus on regions of interest, and peripheral vision, which provides broader contextual awareness across the visual field. Inspired by this dual-process mechanism, as illustrated in Fig. 2, we propose CVP, a 3D scene understanding framework that incorporates two key modules: (1) **target-affinity token**, which functions analogously to central vi-

sion by directing the model’s attention toward question-relevant regions (Sec. 3.1); and (2) **allocentric grid**, which mimics peripheral vision by encoding global scene context and spatial layout from a world-centric perspective (Sec. 3.2). We describe the overall training objective used to jointly optimize these components in Sec. 3.3.

### 3.1. Target-affinity Token

In complex 3D scenes, objects are often densely populated. However, for downstream tasks such as 3D question answering or visual grounding, only a small subset of these objects is typically relevant to the query. The presence of irrelevant objects can introduce semantic noise, distract model attention, and degrade model performance. To mitigate this, we introduce a training mechanism that explicitly teaches the base model to learn focusing on target-relevant regions by incorporating a special supervision token, referred to as the **target-affinity token**.

The target-affinity token is designed to learn the semantic affinity between the objects relevant to input question and objects in the scene. During training, it is supervised using a contrastive objective that encourages alignment with the embeddings of relevant (positive) objects while pushing away embeddings of irrelevant (negative) ones. This mechanism serves as a lightweight, plug-in module that enhances the model’s attention distribution, without requiring additional annotations at inference time.

#### 3.1.1. 3D Object Embedding Extraction

To enable fine-grained affinity modeling between individual objects, we first extract per-object 3D embeddings. Given a multi-view input tensor with  $V$  images  $X \in \mathbb{R}^{V \times 3 \times W \times H}$ , we adopt SigLIP [67] as the vision encoder to obtain 2D features maps:

$$X' = \text{SigLIP}(X), \quad X' \in \mathbb{R}^{V \times C \times W' \times H'}, \quad (1)$$

where  $C$ ,  $W'$ , and  $H'$  denote the feature channel, width, and height, respectively. Each 2D feature map  $X'_i$  from view  $i$  is then back-projected into the shared 3D coordinate space using the known camera intrinsics  $K_i$  and extrinsics  $[R_i \mid t_i]$ . This back-projection operation is consistent with the geometric procedures used in 3D reconstruction systems [13, 69, 73]. Specifically, For each pixel location  $(u, v)$  with depth  $d$ , the corresponding 3D point coordinate  $\mathbf{p} \in \mathbb{R}^3$  is computed as:

$$\mathbf{p} = R_i^{-1}(d K_i^{-1}[u, v, 1]^\top - t_i). \quad (2)$$

The feature vector at  $(u, v)$  from view  $i$  is assigned to its corresponding 3D point  $p$ . By aggregating projected features from all pixels across all  $V$  views, we obtain a 3D point cloud feature set  $P$ .

For each object  $j$  defined by its 3D bounding box, we select the subset of points from  $P$  that lie inside the box.

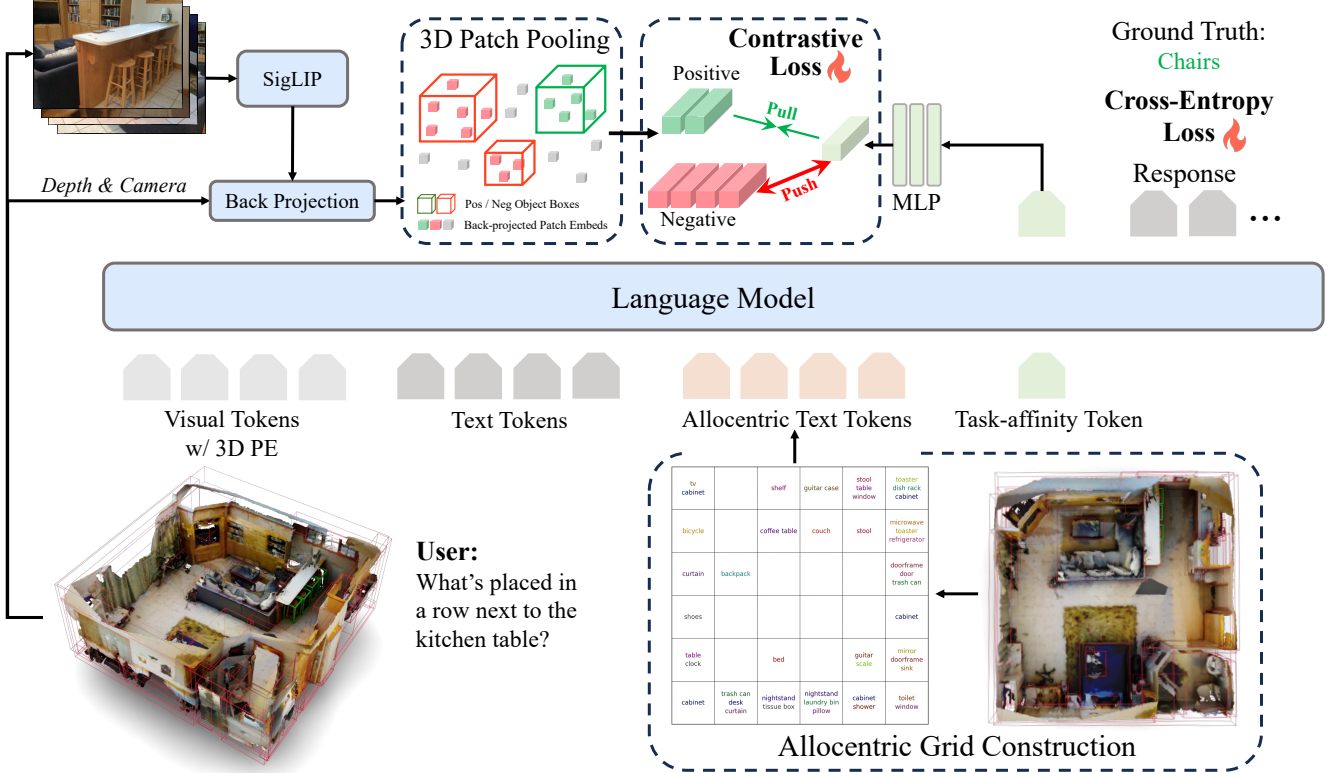


Figure 2. Illustration of CVP. Given visual tokens from multi-view images with 3D positional embeddings and a user question as input, we (1) incorporate a text-based **allocentric grid** to provide allocentric global scene context; and (2) introduce a special **target-affinity token** that guides the model to focus on target-related objects. During output generation, in addition to producing a language response, the representation of the target-affinity token is passed through an MLP and optimized with a contrastive loss against 3D object embeddings back-projected from multi-view 2D features. Positive samples correspond to ground-truth objects relevant to the question, while negatives are irrelevant. This contrastive supervision helps the model attend more effectively to semantically relevant targets.

The per-object embedding  $\mathbf{E}_i$  is then computed via average pooling over the features of these points.

### 3.1.2. Contrastive Learning with Target-affinity Token

To train the model to identify target-relevant objects, we introduce a special target-affinity token to the input of the LLM. During decoding, the model produces a hidden embedding corresponding to this token, and we denote it as  $z_{\text{aff}}$ . Finally,  $z_{\text{aff}}$  is passed through a multi-layer perceptron  $g(\cdot)$  to produce the query vector  $q$ :

$$q = g(z_{\text{aff}}). \quad (3)$$

We then apply the InfoNCE contrastive loss [45], treating embeddings of target-relevant objects as positives and those of irrelevant ones as negatives. Let  $\mathcal{E}_+$  denote the set of positive (question-relevant) object embeddings and  $\mathcal{E}$  the set of all objects. The contrastive objective is defined as:

$$\mathcal{L}_{\text{InfoNCE}} = -\log \frac{\sum_{e_+ \in \mathcal{E}_+} \exp(q^\top e_+ / \tau)}{\sum_{e \in \mathcal{E}} \exp(q^\top e / \tau)}, \quad (4)$$

where  $\tau$  is a temperature hyperparameter. This objective encourages the query embedding  $q$  to be closer (in dot-product similarity) to target-relevant object embeddings  $\mathcal{E}_+$ , while pushing it away from negative ones  $\mathcal{E}_-$ . Details of how we obtain the set of question-relevant object  $\mathcal{E}_+$  are in the supplemental material.

Through this contrastive supervision, the target-affinity token learns to capture the semantic alignment between the question and relevant objects. At inference time, the model with the task-affinity token can shift its attention toward question-aligned content without further supervision.

### 3.2. Allocentric Grid

Understanding the spatial layout of a 3D scene requires not only recognizing individual objects but also reasoning about their spatial relationships, particularly in the vicinity of query-relevant targets. To support this capability, we introduce the allocentric grid, an allocentric (*i.e.*, world-centered) spatial representation that encodes the local neighborhood structure around each object of interest.

In contrast to low-level dense semantic features that en-

code appearance, the allocentric grid emphasizes high-level spatial context, specifically the positions of nearby objects. This representation enables the model to reason about the environment from an allocentric perspective.

We begin by extracting 3D bounding boxes for all objects in the scene and projecting them onto a 2D bird’s-eye-view (BEV) plane. To focus on spatial relationships rather than exact object dimensions, we simplify each object to its BEV center point, discarding size and orientation.

The BEV plane is then partitioned into a uniform grid of discrete cells, each corresponding to a fixed spatial region in the 3D scene. For every object, we identify the cell containing its center and record its category name into the set associated with that cell. This yields a sparse, symbolic world-centric grid, where each cell contains a (possibly empty) set of nearby object names.

To inject this structured spatial context into the model, we convert the allocentric grid into a natural language description. This design ensures full compatibility with the model’s input modality and eliminates the need for additional projection or alignment modules. Specifically, the symbolic contents of the allocentric grid are serialized into a concise spatial summary that expresses the arrangement of objects across grid cells. Please see the supplemental material for the template prompt and other details.

This lightweight textual encoding enables the model to leverage spatial priors while maintaining simplicity and flexibility. Moreover, it complements other input modalities (e.g., RGB images or depth) by enriching the context with high-level allocentric relationships.

### 3.3. Training Objectives

The overall training objective of CVP consists of two components:

- **Language modeling loss**  $\mathcal{L}_{LM}$ , which follows the standard next-token prediction objective for supervising answer generation.
- **Contrastive relevance loss**  $\mathcal{L}_{InfoNCE}$ , described in Sec. 3.1, which encourages the target-affinity token to align with embeddings of question-relevant objects while distancing itself from irrelevant ones.

The final loss is a sum of the two:

$$\mathcal{L}_{total} = \mathcal{L}_{LM} + \mathcal{L}_{InfoNCE}. \quad (5)$$

This objective jointly optimizes both answer generation and object relevance grounding, enabling the model to reason accurately in complex 3D environments.

## 4. Experiments

### 4.1. Experimental Setup

#### 4.1.1. Datasets

We evaluate our model on five 3D scene understanding benchmarks. For 3D visual grounding, we use ScanRefer [7] and Multi3DRefer [70] to assess the models’ object localization capacity given natural language descriptions. For 3D question answering, we incorporate ScanQA [3] and SQA3D [40], which evaluate spatial and situated reasoning capabilities in 3D scenes, respectively. For 3D dense captioning, we include the Scan2Cap [12] benchmark, where the model receives a 3D scene and a target 3D bounding box and is tasked with generating a textual description of the box’s contents. In evaluation, we follow the standard protocol adopted in prior works [11, 21, 74, 76], using the validation sets for Scan2Cap, ScanQA, ScanRefer, and Multi3DRefer, and the test set for SQA3D.

#### 4.1.2. Baselines

To demonstrate the effectiveness of CVP, we compare it with a comprehensive set of baselines across three categories: expert models, 2D large multimodal models (LMMs), and 3D LMMs.

**Expert models.** For 3D visual grounding on ScanRefer and Multi3DRefer, we use baselines including ScanRefer [7], MVT [25], ViL3DRel [8], BUTD-DETR [27], 3DVG-Trans, 3DJCG [6], and M3DRef-CLIP [70]. For question answering on ScanQA and SQA3D, we compare against Scan2Cap [12], ClipBERT [31], MCAN [65], ScanQA [3], and 3D-VisTA [77]. For dense captioning on Scan2Cap, we include Scan2Cap [12], 3DJCG [6], 3D-VLP [29], 3D-VisTA [77], and Vote2Cap-DETR [9] as baselines.

**2D LMMs.** We evaluate against representative large multimodal models including VideoChat2 [34], Qwen2.5-VL-7B [4], and LLaVA-Video [71].

**3D LMMs.** Our comparisons include state-of-the-art 3D LMMs such as 3D-LLM [20], LL3DA [10], Chat-3D v2 [21], Scene-LLM [17], LEO [23], Chat-Scene [22], LLaVA-3D [76], and Video-3D-LLM [74].

#### 4.1.3. Metrics

We use different metrics for the five benchmarks. For Scan2Cap [12] and ScanQA [3], we evaluate metrics include CIDEr [58], BLEU-4 [46], METEOR [5], and ROUGE [37], all of which are at the IoU threshold of 0.5. In addition, we evaluate the exact match accuracy (EM) for ScanQA. For SQA3D [40], we evaluate the EM as well. For ScanRefer [7], we use accuracy at IoU thresholds 0.25 and 0.5. For Multi3DRefer [70], we compute F1 scores at IoU thresholds 0.25 and 0.5.

	ScanRefer		Multi3DRefer	
	Acc@0.25	Acc@0.5	F1@0.25	F1@0.5
<b>Expert models</b>				
ScanRefer [7]	37.3	24.3	—	—
MVT [25]	40.8	33.3	—	—
ViL3DRel [8]	47.9	37.7	—	—
BUTD-DETR [27]	52.2	39.8	—	—
3DVG-Trans [72]	45.9	34.5	—	25.5
3DJCG [6]	49.6	37.3	—	26.6
M3DRef-CLIP [70]	51.0	44.7	42.8	38.4
<b>3D LMMs</b>				
3D-LLM [20]	30.3	—	—	—
Chat-3D v2 [21]	35.9	30.4	—	—
Grounded 3D-LLM [11]	47.9	44.1	45.2	40.6
Chat-Scene [22]	55.5	50.2	57.1	52.4
LLaVA-3D [76]	50.1	42.7	49.8	43.6
Video-3D-LLM [74]	58.1	51.7	58.0	52.7
<b>CVP (Ours)</b>	<b>62.0</b>	<b>55.4</b>	<b>60.2</b>	<b>54.7</b>

Table 1. Quantitative comparison with SOTA models for 3D Visual Grounding task on ScanRefer and Multi3DRefer.

#### 4.1.4. Implementation Details

CVP is built upon LLaVA-Video-7B [71]. We follow the design in Video-3D-LLM [74] that takes multi-view renderings from 3D scenes [14] as an input video to the base model, and replace the original learnable 1D positional embeddings with 3D coordinate embeddings. CVP is fine-tuned for one epoch using a combined training set consisting of five datasets: Scan2Cap [12], ScanQA [3], SQA3D [40], ScanRefer [7], and Multi3DRefer [70].

For training, all videos are downsampled to 3 FPS, with each frame’s corresponding camera intrinsics and extrinsics. The input frame resolution is set to  $384 \times 384$ . We use the AdamW optimizer with a batch size of 8. The warm-up phase spans the first 3% of training steps, during which the learning rate is gradually increased, peaking at  $1e-5$  for the language model and  $2e-6$  for the vision encoder. All experiments are conducted on 8 A100 GPUs.

## 4.2. Comparisons with State-of-the-arts

**Task 1: 3D Visual Grounding.** In Tab. 1, we show results on ScanRefer and Multi3DRefer. CVP achieves state-of-the-art performance across all metrics, surpassing Video-3D-LLM by +3.9 Acc@0.25 and +3.7 Acc@0.5 on ScanRefer, and by +2.2 F1@0.25 and +2.0 F1@0.5 on Multi3DRefer.

**Task 2: 3D Question Answering.** We report the results on 3D question answering benchmarks (ScanQA and SQA3D) in Tab. 2. CVP consistently outperforms the previous state-of-the-art Video-3D-LLM, with improvements of approximately 5–10% across all metrics.

**Task 3: 3D Dense Captioning.** Tab. 3 presents the performance of CVP and baseline methods on Scan2Cap. CVP achieves results comparable to prior state-of-the-art mod-

	ScanQA (val)					SQA3D (test)	
	CIDEr	BLEU-4	METEOR	ROUGE	EM	EM	
<b>Expert models</b>							
Scan2Cap [12]	—	—	—	—	—	—	41.0
ClipBERT [31]	—	—	—	—	—	—	43.3
ScanRefer+MCAN [65]	55.4	7.9	11.5	30.0	18.6	—	—
ScanQA [3]	64.9	10.1	13.1	33.3	21.1	47.2	—
3D-VisTA [77]	69.6	10.4	13.9	35.7	22.4	48.5	—
<b>Zero-shot 2D LMMs</b>							
VideoChat2 [34]	49.2	9.6	9.5	28.2	19.2	37.3	—
Qwen2.5-VL-7B [4]	53.9	3.0	11.4	29.3	—	46.5	—
LLaVA-Video [71]	88.7	3.1	17.7	44.6	—	48.5	—
<b>3D LMMs</b>							
3D-LLM [20]	69.4	12.0	14.5	35.7	20.5	—	—
LL3DA [10]	76.8	13.5	15.9	37.3	—	—	—
Chat-3D v2 [21]	87.6	14.0	—	—	—	54.7	—
Scene-LLM [17]	80.0	12.0	16.6	40.0	27.2	54.2	—
LEO [23]	101.4	13.2	20.0	49.2	24.5	50.0	—
Chat-Scene [22]	87.7	14.3	18.0	41.6	21.6	54.6	—
LLaVA-3D [76]	91.7	14.5	20.7	50.1	27.0	55.6	—
Video-3D-LLM [74]	102.1	16.2	19.8	49.0	30.1	58.6	—
<b>CVP (Ours)</b>	<b>107.1</b>	<b>17.8</b>	<b>20.8</b>	<b>50.9</b>	<b>31.2</b>	<b>62.3</b>	—

Table 2. Quantitative comparisons with SOTA models for 3D Question Answering task on ScanQA and SQA3D.

	Scan2Cap (Val)			
	CIDEr	BLEU-4	METEOR	ROUGE
<b>Expert models</b>				
Scan2Cap [12]	39.1	23.3	22.0	44.8
3DJCG [6]	49.5	31.0	24.2	50.8
3D-VLP [29]	55.0	32.3	24.8	51.5
3D-VisTA [77]	61.6	34.1	26.8	55.0
Vote2Cap-DETR [9]	61.8	34.5	26.2	54.4
<b>3D LMMs</b>				
LL3DA [10]	65.2	36.8	26.0	55.0
LEO [23]	68.4	36.9	27.7	57.8
Chat-Scene [22]	77.2	36.3	28.0	58.1
LLaVA-3D [76]	79.2	41.1	30.2	63.4
Video-3D-LLM [74]	83.8	41.3	28.9	62.3
<b>CVP (Ours)</b>	<b>90.5</b>	<b>41.7</b>	28.9	62.2

Table 3. Quantitative comparisons with SOTA models for 3D Dense Captioning task on Scan2Cap.

els such as LLaVA-3D and Video-3D-LLM in terms of METEOR and ROUGE, while surpassing them on CIDEr (+6.7) and BLEU-4 (+0.4).

Overall, CVP consistently outperforms existing methods across tasks and metrics, demonstrating the effectiveness of our proposed designs.

## 4.3. Ablation Study

We provide ablation studies on the proposed Allocentric Grid and Target-affinity Token in Tab. 4.

**Allocentric Grid and Target-affinity Token.** Section a) of Tab. 4 show the ablation results when each of the two proposed modules is removed individually. Performance drops in both cases, confirming the contribution of each component. The target-affinity token provides a more significant boost in visual grounding tasks by improving model’s ob-

Ablation Setting	Scan2Cap		ScanQA		SQA3D		ScanRefer		Multi3DRef	
	BLEU-4	CIDEr	CIDEr	EM	EM	Acc@0.25	Acc@0.5	F1@0.25	F1@0.5	
CVP	41.7	90.5	107.1	31.2	62.3	62.0	55.4	60.2	54.7	
<b>a) without...</b>										
Allocentric Grid	41.3	84.4	103.9	30.0	59.2	62.0	55.1	59.9	54.6	
Target-affinity Token	40.8	85.8	107.6	31.5	62.2	59.5	53.0	58.7	53.3	
<b>b) Allocentric Grid setting</b>										
Grid Size = 10	41.4	85.8	104.8	30.3	59.6	61.5	55.0	60.1	54.7	
Grid Size = 16	42.2	88.8	102.8	29.7	58.8	61.7	55.1	60.0	54.5	
Grid Size = 24	42.1	87.3	102.7	30.0	58.8	61.9	55.3	59.7	54.2	
Replace texts w/ embeddings	41.9	86.1	103.6	30.0	59.1	61.8	55.3	59.9	54.6	
<b>c) Target-affinity Token setting</b>										
Contrastive $\rightarrow$ Regression	40.8	86.3	106.7	31.5	59.8	59.0	52.7	59.1	53.7	
GT Boxes $\rightarrow$ All Related Boxes	40.3	79.6	98.7	28.4	57.1	57.2	51.0	56.3	51.3	

Table 4. Ablation studies on Allocentric Grid and Target-affinity Token and their respective settings.

ject localization capacity. In contrast, the allocentric grid offers greater benefits for dense captioning and question answering by supplying high-level abstractions of the 3D environment, enhancing overall scene understanding.

**Allocentric Grid Size.** We ablate different settings of allocentric grid in Section b) of Tab. 4. We first expanding the default  $6 \times 6$  grid to  $10 \times 10$ ,  $16 \times 16$ , and  $24 \times 24$  layouts. Finer grids could minimize the chance of multiple objects sharing a single cell, and more precisely represent the layout of 3D scenes. However, the results show no performance gains from higher-resolution grids. We suspect that coarser, more abstract grids provide clearer structural cues, while overly detailed grids introduce unnecessary complexity that hinders scene understanding for the model.

**Allocentric Grid Object Representation.** By default, we represent allocentric grids with text, directly incorporating object names as textual elements. To examine whether an “object-centric” design, as in prior works [21–23], improves performance, we replace object names with embeddings extracted from the input video using a pretrained vision encoder, followed by pooling, identical to the embeddings used for target-affinity tokens. As shown by the last row of Section b) in Tab. 4, this embedding-based variant underperforms our text-only design. We attribute this to modality mismatch: vision-derived embeddings introduce alignment errors, which are further amplified by 3D aggregation, whereas text tokens are compatible with the base model.

**Target-affinity Token Settings.** In Section c) of Tab. 4, We ablate two alternative designs for our target-affinity token. We first replace the InfoNCE contrastive loss with a mean squared error (MSE) loss for direct regression, and the experiment show that this modification yields poorer performance. We also experiment with using all related boxes for supervision instead of just the ground-truth box. Con-

cretely, we parse each training sample’s questions and answers to identify every referenced object, then label every bounding box matching those names in the 3D scene as relevant. However, this modification results in a significant decline in performance. We attribute this to the increased ambiguity introduced by multiple instances of the same object category, which can confuse the model and degrade the precision of attention.

#### 4.4. Visualizations

We showcase the effectiveness of the target-affinity token through an object retrieval task. Specifically, we compute embeddings for all objects in the scene (as described earlier), and retrieve those most similar to the output target-affinity embedding. Representative results are shown in Fig. 3. The top-1 retrieved object consistently matches the one referred to in the user query. The top-3 results often include semantically related objects (e.g., a trash can at the bottom left) and spatially adjacent instances (e.g., a nearby cabinet), illustrating that the target-affinity token embedding effectively captures information relevant to the current question and its potential answers.



Figure 3. Object retrieval results using our target-affinity token. We compute similarities between the output target-affinity embedding and all object embeddings in the scene. The top-1 result is shown in a green box; top-3 results are highlighted in orange.

**3D Dense Captioning**



**User:**  
Given an object located at <coord>, describe the object in detail.

**Ground-Truth:**  
This is a white soap dispenser mounted on the wall to the right of the sinks.

**Video-3D-LLM:**  
This is a white sink. It is to the right of the door.

**CVP:**  
This is a white soap dispenser. It is to the right of the sink.

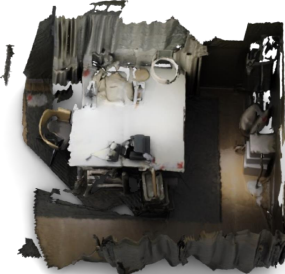
**3D Visual Grounding**



**User:**  
Identify the object according to the following description. The kitchen sink is to the left of the refrigerator which is located closest to the left side of the room.

**GT**      **Video-3D-LLM**      **Retrieved Top1**      **Retrieved Top2**      **Retrieved Top3**

**3D Question Answering**



	curtain			rack
	table	lamp		
chair			box	
		tray rack	stand	
				curtain

Allocentric Grid

**Ground-Truth:**  
Tray rack.

**Video-3D-LLM:**  
Sewing Machine.

**CVP:**  
Tray rack.

Figure 4. Qualitative comparisons across three representative 3D vision-language tasks: dense captioning, visual grounding, and question answering. CVP consistently outperforms the baseline model.

We also present visualization of the three 3D spatial understanding tasks in Fig. 4:

- **3D Dense Captioning.** Given the object location, Video-3D-LLM mistakes a nearby white sink for the target soap dispenser. In contrast, CVP accurately describes the soap dispenser. The improvement comes from the target-affinity token, which helps focus on the correct object.
- **3D Visual Grounding.** When asked to identify the kitchen sink relative to the refrigerator, Video-3D-LLM selects the wrong region. CVP successfully grounds the correct object. It leverages retrieved candidates and spatial language cues to resolve the relational instruction.
- **3D Question Answering.** The model is queried about an object near the table and in front of a curtain. Video-3D-LLM responds with “sewing machine”, which violates the spatial constraint. CVP outputs “tray rack” by

reasoning over the allocentric grid.

## 5. Conclusion

We present CVP, a 3D scene understanding framework inspired by components of the human visual field. CVP introduces two new key mechanisms: the target-affinity token that guides the model’s attention toward target objects, analogous to central vision for fine-grained perception; and the allocentric grid, which captures global scene context and spatial relationships, akin to peripheral vision. These complementary components enable structured, context-aware reasoning in complex 3D environments. Extensive experiments across multiple benchmarks demonstrate that CVP achieves state-of-the-art performance.

8

## Acknowledgment

This work is supported by NSF award IIS-2127544 and NSF award IIS-2433768. We thank Lambda, Inc. for their compute resource help.

## References

- [1] Josh Achiam, Steven Adler, Sandhini Agarwal, Lama Ahmad, Ilge Akkaya, Florencia Leoni Aleman, Diogo Almeida, Janko Altenschmidt, Sam Altman, Shyamal Anadkat, et al. Gpt-4 technical report. *arXiv preprint arXiv:2303.08774*, 2023. [1](#), [2](#)
- [2] Panos Achlioptas, Ahmed Abdelreheem, Fei Xia, Mohamed Elhoseiny, and Leonidas Guibas. Referit3d: Neural listeners for fine-grained 3d object identification in real-world scenes. In *ECCV*, pages 422–440. Springer, 2020. [2](#)
- [3] Daichi Azuma, Taiki Miyanishi, Shuhei Kurita, and Motoaki Kawanabe. Scanqa: 3d question answering for spatial scene understanding. In *CVPR*, pages 19129–19139, 2022. [1](#), [2](#), [5](#), [6](#), [12](#)
- [4] Shuai Bai, Keqin Chen, Xuejing Liu, Jialin Wang, Wenbin Ge, Sibo Song, Kai Dang, Peng Wang, Shijie Wang, Jun Tang, et al. Owen2. 5-vl technical report. *arXiv preprint arXiv:2502.13923*, 2025. [2](#), [5](#)
- [5] Satanjeev Banerjee and Alon Lavie. Meteor: An automatic metric for mt evaluation with improved correlation with human judgments. In *ACL workshop on intrinsic and extrinsic evaluation measures for machine translation and/or summarization*, 2005. [5](#)
- [6] Daigang Cai, Lichen Zhao, Jing Zhang, Lu Sheng, and Dong Xu. 3djcg: A unified framework for joint dense captioning and visual grounding on 3d point clouds. In *CVPR*, pages 16464–16473, 2022. [5](#), [6](#)
- [7] Dave Zhenyu Chen, Angel X Chang, and Matthias Nießner. Scanrefer: 3d object localization in rgb-d scans using natural language. In *ECCV*, pages 202–221. Springer, 2020. [1](#), [2](#), [5](#), [6](#), [12](#)
- [8] Shizhe Chen, Pierre-Louis Guhur, Makarand Tapaswi, Cordelia Schmid, and Ivan Laptev. Language conditioned spatial relation reasoning for 3d object grounding. *NeurIPS*, 35:20522–20535, 2022. [2](#), [5](#), [6](#)
- [9] Sijin Chen, Hongyuan Zhu, Xin Chen, Yinjie Lei, Gang Yu, and Tao Chen. End-to-end 3d dense captioning with vote2cap-detr. In *CVPR*, pages 11124–11133, 2023. [5](#), [6](#)
- [10] Sijin Chen, Xin Chen, Chi Zhang, Mingsheng Li, Gang Yu, Hao Fei, Hongyuan Zhu, Jiayuan Fan, and Tao Chen. Ll3da: Visual interactive instruction tuning for omni-3d understanding reasoning and planning. In *CVPR*, pages 26428–26438, 2024. [2](#), [3](#), [5](#), [6](#)
- [11] Yilun Chen, Shuai Yang, Haifeng Huang, Tai Wang, Runsen Xu, Ruiyuan Lyu, Dahua Lin, and Jiangmiao Pang. Grounded 3d-llm with referent tokens. *arXiv preprint arXiv:2405.10370*, 2024. [3](#), [5](#)
- [12] Zhenyu Chen, Ali Gholami, Matthias Nießner, and Angel X Chang. Scan2cap: Context-aware dense captioning in rgb-d scans. In *CVPR*, pages 3193–3203, 2021. [1](#), [2](#), [5](#), [6](#), [12](#)
- [13] Manuel Dahnert, Ji Hou, Matthias Nießner, and Angela Dai. Panoptic 3d scene reconstruction from a single rgb image. *NeurIPS*, 34:8282–8293, 2021. [3](#)
- [14] Angela Dai, Angel X Chang, Manolis Savva, Maciej Halber, Thomas Funkhouser, and Matthias Nießner. Scannet: Richly-annotated 3d reconstructions of indoor scenes. In *CVPR*, pages 5828–5839, 2017. [6](#)
- [15] Sheng Fan, Rui Liu, Wenguan Wang, and Yi Yang. Navigation instruction generation with bev perception and large language models. In *ECCV*, 2024. [2](#)
- [16] Luciano Floridi and Massimo Chiriatti. Gpt-3: Its nature, scope, limits, and consequences. *Minds and machines*, 2020. [1](#)
- [17] Rao Fu, Jingyu Liu, Xilun Chen, Yixin Nie, and Wenhao Xiong. Scene-llm: Extending language model for 3d visual understanding and reasoning. *arXiv preprint arXiv:2403.11401*, 2024. [5](#), [6](#)
- [18] Xiaoning Han, Shuailong Li, Xiaohui Wang, and Weijia Zhou. Semantic mapping for mobile robots in indoor scenes: A survey. *Information*, 12(2):92, 2021. [1](#)
- [19] Tairan He, Jiawei Gao, Wenli Xiao, Yuanhang Zhang, Zi Wang, Jiashun Wang, Zhengyi Luo, Guanqi He, Nikhil Sobanbab, Chaoyi Pan, et al. Asap: Aligning simulation and real-world physics for learning agile humanoid whole-body skills. *arXiv preprint arXiv:2502.01143*, 2025. [1](#)
- [20] Yining Hong, Haoyu Zhen, Peihao Chen, Shuhong Zheng, Yilun Du, Zhenfang Chen, and Chuang Gan. 3d-llm: Injecting the 3d world into large language models. *NeurIPS*, 36: 20482–20494, 2023. [2](#), [3](#), [5](#), [6](#)
- [21] Haifeng Huang, Zehan Wang, Rongjie Huang, Luping Liu, Xize Cheng, Yang Zhao, Tao Jin, and Zhou Zhao. Chat-3d v2: Bridging 3d scene and large language models with object identifiers. *arXiv preprint arXiv:2312.08168*, 2023. [2](#), [3](#), [5](#), [6](#), [7](#)
- [22] Haifeng Huang, Yilun Chen, Zehan Wang, Rongjie Huang, Runsen Xu, Tai Wang, Luping Liu, Xize Cheng, Yang Zhao, Jiangmiao Pang, et al. Chat-scene: Bridging 3d scene and large language models with object identifiers. *NeurIPS*, 37: 113991–114017, 2024. [5](#), [6](#)
- [23] Jiangyong Huang, Silong Yong, Xiaojian Ma, Xiongkun Linghu, Puha Li, Yan Wang, Qing Li, Song-Chun Zhu, Baoxiong Jia, and Siyuan Huang. An embodied generalist agent in 3d world. In *ICML*, pages 20413–20451, 2024. [2](#), [3](#), [5](#), [6](#), [7](#)
- [24] Shijia Huang, Yilun Chen, Jiaya Jia, and Liwei Wang. Multi-view transformer for 3d visual grounding. In *CVPR*, pages 15524–15533, 2022. [2](#)
- [25] Shijia Huang, Yilun Chen, Jiaya Jia, and Liwei Wang. Multi-view transformer for 3d visual grounding. In *CVPR*, pages 15524–15533, 2022. [2](#), [5](#), [6](#)
- [26] Aaron Hurst, Adam Lerer, Adam P Goucher, Adam Perelman, Aditya Ramesh, Aidan Clark, AJ Ostrow, Akila Welihinda, Alan Hayes, Alec Radford, et al. Gpt-4o system card. *arXiv preprint arXiv:2410.21276*, 2024. [12](#)
- [27] Ayush Jain, Nikolaos Gkanatsios, Ishita Mediratta, and Katherine Fragkiadaki. Bottom up top down detection transformers for language grounding in images and point clouds. In *ECCV*, pages 417–433. Springer, 2022. [2](#), [5](#), [6](#)

[28] Yang Jiao, Shaoxiang Chen, Zequn Jie, Jingjing Chen, Lin Ma, and Yu-Gang Jiang. More: Multi-order relation mining for dense captioning in 3d scenes. In *ECCV*, pages 528–545. Springer, 2022. 2

[29] Zhao Jin, Munawar Hayat, Yuwei Yang, Yulan Guo, and Yinjie Lei. Context-aware alignment and mutual masking for 3d-language pre-training. In *CVPR*, pages 10984–10994, 2023. 5, 6

[30] Alex H Lang, Sourabh Vora, Holger Caesar, Lubing Zhou, Jiong Yang, and Oscar Beijbom. Pointpillars: Fast encoders for object detection from point clouds. In *CVPR*, pages 12697–12705, 2019. 1, 2

[31] Jie Lei, Linjie Li, Luowei Zhou, Zhe Gan, Tamara L Berg, Mohit Bansal, and Jingjing Liu. Less is more: Clipbert for video-and-language learning via sparse sampling. In *CVPR*, pages 7331–7341, 2021. 5, 6

[32] Bo Li, Yuanhan Zhang, Dong Guo, Renrui Zhang, Feng Li, Hao Zhang, Kaichen Zhang, Peiyuan Zhang, Yanwei Li, Ziwei Liu, and Chunyuan Li. LLaVA-onevision: Easy visual task transfer. *TMLR*, 2025. 2

[33] Junnan Li, Dongxu Li, Silvio Savarese, and Steven Hoi. Blip-2: Bootstrapping language-image pre-training with frozen image encoders and large language models. In *ICML*, 2023. 2, 3

[34] Kunchang Li, Yali Wang, Yinan He, Yizhuo Li, Yi Wang, Yi Liu, Zun Wang, Jilan Xu, Guo Chen, Ping Luo, et al. Mvbench: A comprehensive multi-modal video understanding benchmark. In *CVPR*, pages 22195–22206, 2024. 5, 6

[35] Xin Li, Zequn Jie, Wei Wang, Changsong Liu, Jimei Yang, Xiaohui Shen, Zhe Lin, Qiang Chen, Shuicheng Yan, and Jiashi Feng. Foveanet: Perspective-aware urban scene parsing. In *ICCV*, pages 784–792, 2017. 2

[36] Zechuan Li, Hongshan Yu, Yihao Ding, Yan Li, Yong He, and Naveed Akhtar. Embodied intelligence for 3d understanding: A survey on 3d scene question answering. *arXiv preprint arXiv:2502.00342*, 2025. 1

[37] Chin-Yew Lin. Rouge: A package for automatic evaluation of summaries. In *Text summarization branches out*, 2004. 5

[38] Aixin Liu, Bei Feng, Bing Xue, Bingxuan Wang, Bochao Wu, Chengda Lu, Chenggang Zhao, Chengqi Deng, Chenyu Zhang, Chong Ruan, et al. Deepseek-v3 technical report. *arXiv preprint arXiv:2412.19437*, 2024. 1

[39] Haotian Liu, Chunyuan Li, Qingyang Wu, and Yong Jae Lee. Visual instruction tuning. *NeurIPS*, 36:34892–34916, 2023. 2

[40] Xiaojian Ma, Silong Yong, Zilong Zheng, Qing Li, Yitao Liang, Song-Chun Zhu, and Siyuan Huang. Sqa3d: Situated question answering in 3d scenes. In *ICLR*, 2023. 1, 2, 5, 6, 12

[41] Yunze Man, Liang-Yan Gui, and Yu-Xiong Wang. Situational awareness matters in 3d vision language reasoning. In *CVPR*, pages 13678–13688, 2024. 2

[42] Chen Min, Dawei Zhao, Liang Xiao, Jian Zhao, Xinli Xu, Zheng Zhu, Lei Jin, Jianshu Li, Yulan Guo, Junliang Xing, et al. Driveworld: 4d pre-trained scene understanding via world models for autonomous driving. In *CVPR*, pages 15522–15533, 2024. 1

[43] Khan Muhammad, Tanveer Hussain, Hayat Ullah, Javier Del Ser, Mahdi Rezaei, Neeraj Kumar, Mohammad Hiji, Paolo Bellavista, and Victor Hugo C De Albuquerque. Vision-based semantic segmentation in scene understanding for autonomous driving: Recent achievements, challenges, and outlooks. *IEEE Transactions on Intelligent Transportation Systems*, 23(12):22694–22715, 2022. 1

[44] Richard A Newcombe, Shahram Izadi, Otmar Hilliges, David Molyneaux, David Kim, Andrew J Davison, Pushmeet Kohi, Jamie Shotton, Steve Hodges, and Andrew Fitzgibbon. Kinectfusion: Real-time dense surface mapping and tracking. In *IEEE international symposium on mixed and augmented reality*, pages 127–136, 2011. 1, 2

[45] Aaron van den Oord, Yazhe Li, and Oriol Vinyals. Representation learning with contrastive predictive coding. *arXiv preprint arXiv:1807.03748*, 2018. 4

[46] Kishore Papineni, Salim Roukos, Todd Ward, and Wei-Jing Zhu. Bleu: a method for automatic evaluation of machine translation. In *ACL*, 2002. 5

[47] Maria Parelli, Alexandros Delitzas, Nikolas Hars, Georgios Vlassis, Sotirios Anagnostidis, Gregor Bachmann, and Thomas Hofmann. Clip-guided vision-language pre-training for question answering in 3d scenes. In *CVPR*, pages 5607–5612, 2023. 2

[48] Charles R Qi, Wei Liu, Chenxia Wu, Hao Su, and Leonidas J Guibas. Frustum pointnets for 3d object detection from rgbd data. In *CVPR*, pages 918–927, 2018. 1, 2

[49] Alec Radford, Jong Wook Kim, Chris Hallacy, Aditya Ramesh, Gabriel Goh, Sandhini Agarwal, Girish Sastry, Amanda Askell, Pamela Mishkin, Jack Clark, et al. Learning transferable visual models from natural language supervision. In *ICML*, 2021. 3

[50] Adria Recasens, Petr Kellnhofer, Simon Stent, Wojciech Matusik, and Antonio Torralba. Learning to zoom: a saliency-based sampling layer for neural networks. In *ECCV*, pages 51–66, 2018. 2

[51] Renato F Salas-Moreno, Richard A Newcombe, Hauke Strasdat, Paul HJ Kelly, and Andrew J Davison. Slam++: Simultaneous localisation and mapping at the level of objects. In *CVPR*, pages 1352–1359, 2013. 1, 2

[52] Gemini Team, Rohan Anil, Sebastian Borgeaud, Jean-Baptiste Alayrac, Jiahui Yu, Radu Soricut, Johan Schalkwyk, Andrew M Dai, Anja Hauth, Katie Millican, et al. Gemini: a family of highly capable multimodal models. *arXiv preprint arXiv:2312.11805*, 2023. 1, 2

[53] Gemini Team, Petko Georgiev, Ving Ian Lei, Ryan Burnell, Libin Bai, Anmol Gulati, Garrett Tanzer, Damien Vincent, Zhufeng Pan, Shibo Wang, et al. Gemini 1.5: Unlocking multimodal understanding across millions of tokens of context. *arXiv preprint arXiv:2403.05530*, 2024. 2

[54] Chittesh Thavamani, Mengtian Li, Nicolas Cebron, and Deva Ramanan. Fovea: Foveated image magnification for autonomous navigation. In *ICCV*, pages 15539–15548, 2021. 2

[55] Sebastian Thrun. Probabilistic robotics. *Communications of the ACM*, 45(3):52–57, 2002. 1, 2

[56] Hugo Touvron, Thibaut Lavril, Gautier Izacard, Xavier Martinet, Marie-Anne Lachaux, Timothée Lacroix, Baptiste

Rozière, Naman Goyal, Eric Hambro, Faisal Azhar, et al. Llama: Open and efficient foundation language models. *arXiv preprint arXiv:2302.13971*, 2023. 1

[57] Hugo Touvron, Louis Martin, Kevin Stone, Peter Albert, Amjad Almahairi, Yasmine Babaei, Nikolay Bashlykov, Soumya Batra, Prajjwal Bhargava, Shruti Bhosale, et al. Llama 2: Open foundation and fine-tuned chat models. *arXiv preprint arXiv:2307.09288*, 2023. 1

[58] Ramakrishna Vedantam, C Lawrence Zitnick, and Devi Parikh. Cider: Consensus-based image description evaluation. In *CVPR*, pages 4566–4575, 2015. 5

[59] Zihan Wang and Gim Hee Lee. g3d-lf: Generalizable 3d-language feature fields for embodied tasks. In *CVPR*, 2025. 2

[60] Zehan Wang, Haifeng Huang, Yang Zhao, Linjun Li, Xize Cheng, Yichen Zhu, Aoxiong Yin, and Zhou Zhao. 3drp-net: 3d relative position-aware network for 3d visual grounding. In *EMNLP*, 2023. 2

[61] Yanmin Wu, Xinhua Cheng, Renrui Zhang, Zesen Cheng, and Jian Zhang. Eda: Explicit text-decoupling and dense alignment for 3d visual grounding. In *CVPR*, pages 19231–19242, 2023. 2

[62] Runsen Xu, Xiaolong Wang, Tai Wang, Yilun Chen, Jiangmiao Pang, and Dahua Lin. Pointlm: Empowering large language models to understand point clouds. In *ECCV*, pages 131–147. Springer, 2024. 3

[63] Yuncong Yang, Han Yang, Jiachen Zhou, Peihao Chen, Hongxin Zhang, Yilun Du, and Chuang Gan. 3d-mem: 3d scene memory for embodied exploration and reasoning. In *CVPR*, pages 17294–17303, 2025. 1

[64] Xumin Yu, Lulu Tang, Yongming Rao, Tiejun Huang, Jie Zhou, and Jiwen Lu. Point-bert: Pre-training 3d point cloud transformers with masked point modeling. In *CVPR*, pages 19313–19322, 2022. 2, 3

[65] Zhou Yu, Jun Yu, Yuhao Cui, Dacheng Tao, and Qi Tian. Deep modular co-attention networks for visual question answering. In *CVPR*, pages 6281–6290, 2019. 5, 6

[66] Zhihao Yuan, Xu Yan, Yinghong Liao, Yao Guo, Guanbin Li, Shuguang Cui, and Zhen Li. X-trans2cap: Cross-modal knowledge transfer using transformer for 3d dense captioning. In *CVPR*, pages 8563–8573, 2022. 2

[67] Xiaohua Zhai, Basil Mustafa, Alexander Kolesnikov, and Lucas Beyer. Sigmoid loss for language image pre-training. In *ICCV*, pages 11975–11986, 2023. 3

[68] Renrui Zhang, Ziyu Guo, Wei Zhang, Kunchang Li, Xupeng Miao, Bin Cui, Yu Qiao, Peng Gao, and Hongsheng Li. Pointclip: Point cloud understanding by clip. In *CVPR*, pages 8552–8562, 2022. 2

[69] Xiang Zhang, Zeyuan Chen, Fangyin Wei, and Zhuowen Tu. Uni-3d: A universal model for panoptic 3d scene reconstruction. In *ICCV*, pages 9256–9266, 2023. 3

[70] Yiming Zhang, ZeMing Gong, and Angel X Chang. Multi3drefrer: Grounding text description to multiple 3d objects. In *ICCV*, pages 15225–15236, 2023. 1, 2, 5, 6, 12

[71] Yuanhan Zhang, Jinming Wu, Wei Li, Bo Li, Zejun Ma, Ziwei Liu, and Chunyuan Li. Video instruction tuning with synthetic data. *arXiv preprint arXiv:2410.02713*, 2024. 2, 5, 6

[72] Lichen Zhao, Daigang Cai, Lu Sheng, and Dong Xu. 3dvg-transformer: Relation modeling for visual grounding on point clouds. In *ICCV*, pages 2928–2937, 2021. 6

[73] Qingcheng Zhao, Xiang Zhang, Haiyang Xu, Zeyuan Chen, Jianwen Xie, Yuan Gao, and Zhuowen Tu. Depr: Depth guided single-view scene reconstruction with instance-level diffusion. In *ICCV*, pages 5722–5733, 2025. 3

[74] Duo Zheng, Shijia Huang, and Liwei Wang. Video-3d llm: Learning position-aware video representation for 3d scene understanding. In *CVPR*, pages 8995–9006, 2025. 1, 2, 3, 5, 6, 12

[75] Yin Zhou and Oncel Tuzel. Voxelenet: End-to-end learning for point cloud based 3d object detection. In *CVPR*, pages 4490–4499, 2018. 1, 2

[76] Chenming Zhu, Tai Wang, Wenwei Zhang, Jiangmiao Pang, and Xihui Liu. Llava-3d: A simple yet effective pathway to empowering llms with 3d capabilities. In *ICCV*, pages 4295–4305, 2025. 1, 2, 3, 5, 6

[77] Ziyu Zhu, Xiaojian Ma, Yixin Chen, Zhidong Deng, Siyuan Huang, and Qing Li. 3d-vista: Pre-trained transformer for 3d vision and text alignment. In *ICCV*, pages 2911–2921, 2023. 5, 6

[78] Ziyu Zhu, Xilin Wang, Yixuan Li, Zhuofan Zhang, Xiaojian Ma, Yixin Chen, Baoxiong Jia, Wei Liang, Qian Yu, Zhidong Deng, et al. Move to understand a 3d scene: Bridging visual grounding and exploration for efficient and versatile embodied navigation. In *ICCV*, pages 8120–8132, 2025. 1

## A. Appendix

Benchmarks	Scan2Cap				ScanQA					SQA3D	
	CIDEr	BLEU-4	METEOR	ROUGE	CIDEr	BLEU-4	METEOR	ROUGE	EM	EM	
GPT-4o [26]	7.0	5.5	17.1	38.5	43.3	16.6	16.3	31.6	11.1	41.7	
CVP	90.5	41.7	28.9	62.2	107.1	17.8	20.8	50.9	31.2	62.3	

Table A.1. Comparison between GPT-4o and CVP across Scan2Cap, ScanQA, and SQA3D benchmarks.

### A.1. Implementation Details

#### A.1.1. Evaluation with GPT Model

To compare with strong closed-source systems, we evaluate GPT-4o [26] on the benchmarks used in the main paper. Following the same strategy as CVP and Video-3D-LLM [74], we uniformly extract frames from the scene videos as input to generate visual tokens. Since GPT-4o produces only text output, it is largely unable to predict the 3D bounding-box coordinates required by the referring benchmarks (ScanRefer [7] and Multi3DRefer [70]). Therefore, we report its performance only on Scan2Cap [12], ScanQA [3], and SQA3D [40]. As shown in Table A.1, without task-specific fine-tuning, even the powerful GPT-4o model falls short of the spatial understanding demonstrated by specialized models such as our proposed CVP. This gap is particularly evident on the Scan2Cap [12] benchmark, where precise object localization based on coordinate inputs is essential.

#### A.1.2. Task Relevant Objects

We describe how target objects are identified and task-relevant object sets  $\mathcal{E}_+$  are constructed from the five training datasets.

In ScanRefer [7], each question is linked to one specific object from the given 3D scene. We directly use this object as the target object.

For Multi3DRefer [70], each question may refer to zero, one, or multiple objects in the 3D scene. Consequently, the number of target objects for a sample from this dataset ranges from zero to several instances.

In Scan2Cap [12], the model is tasked to give a precise description for a single referring object, with its 3D bounding box provided as input. Since the dataset provides the metadata of the object to be described for each data sample, we assign that object as the target.

ScanQA [3] provides a large collection of QA pairs, each accompanied by an object ID list and a corresponding name list of all objects relevant to the pair. Since some samples include multiple objects from different categories and distant locations, which may impede the learning of our task-affinity token, we apply a filtering strategy. Specifically, we retain only cases where (1) the object list contains a single instance, or (2) all object names are identical and matches

the answer, which commonly occurs in questions such as “What is to the left of the chair?”.

SQA3D [40] benchmarks the situated Question Answering task in 3D Scenes. It does not provide corresponding objects to their QA pairs. Therefore, we do not compute the InfoNCE loss for the task-affinity token when training on its samples.

#### A.1.3. Allocentric Grid Prompt Template

Given a set of 3D object bounding boxes, we retain their x- and y-axis coordinates and discretize them to place all objects into our allocentric grid. The grid is first represented as a dictionary, where each key corresponds to a 2D grid cell coordinate  $(x, y)$  and the value is the list of object names located in that cell. This dictionary is then used to populate the following text prompt:

This is a top-down view of a scene divided into a  $\{\text{grid\_H}\}$  by  $\{\text{grid\_W}\}$  grid. Each cell may contain multiple objects, and the objects are separated by commas. This is an abstraction of the scene and might be incomplete.

At  $(\text{row}=\{x\}, \text{col}=\{y\})$ , there is:  $\{\text{obj\_str}\}$ ,  
At  $(\text{row}=\{x\}, \text{col}=\{y\})$ , there is:  $\{\text{obj\_str}\}$ ,  
...